Research article

Dandan Han, Changhoon Park, Seonghyeon Oh, Howon Jung and Jae W. Hahn*

Quantitative analysis and modeling of line edge roughness in near-field lithography: toward high pattern quality in nanofabrication

https://doi.org/10.1515/nanoph-2019-0031
Received February 4, 2019; revised March 23, 2019; accepted April 1, 2019

Abstract: Quantitative analysis of line edge roughness (LER) is very important for understanding the root causes of LER and thereby improving the pattern quality in near-field lithography (NFL), because LER has become the main limiter of critical dimension (CD) control as the feature size of nanostructures is scaled down. To address this challenge, the photoresist point-spread function of NFL with a contact plasmonic ridge nanoaperture can be employed to account for the physical and chemical effects involved in the LER-generation mechanism. Our theoretical and experimental results show that the sources of LER in NFL mainly come from the aerial image, material chemistry, and process. Importantly, the complicated decay characteristics of surface plasmon waves are demonstrated to be the main optical contributor. Because the evanescent mode of surface plasmon polaritons (SPPs) and quasi-spherical waves (QSWs) decay in the lateral direction, they can induce a small image log-slope and low photoresist contrast, leading to a large LER. We introduce an analytical model and demonstrate the relationship between LER and CD to estimate the pattern quality in NFL. We expect that these results can provide alternative approaches to further improve pattern uniformity and resolution, which can lead to advanced nanopatterning results in NFL.

***Corresponding author: Jae W. Hahn,** Nano Photonics Laboratory, School of Mechanical Engineering, Yonsei University, 50 Yonsei-ro, Seodaemun-gu, Seoul, 120-749, Republic of Korea, e-mail: jaewhahn@yonsei.ac.kr. https://orcid.org/0000-0003-2745-9973
Dandan Han, Changhoon Park, Seonghyeon Oh and Howon Jung: Nano Photonics Laboratory, School of Mechanical Engineering, Yonsei University, 50 Yonsei-ro, Seodaemun-gu, Seoul, 120-749, Republic of Korea

Keywords: line edge roughness; near-field lithography; surface plasmon waves; image log-slope; resist contrast; point-spread function.

1 Introduction

Near-field lithography (NFL) is a sub-diffraction-limited nanopatterning technology by exploiting surface plasmon polaritons (SPPs) and the diffracted field such as quasi-spherical waves (QSWs) [1–20]. These waves are excited by an incident light and confined in the horizontal plane and the perpendicular direction through strong near-field coupling via evanescent photons. As an alternative low-cost nanofabrication, the pattern resolution of NFL has been successfully demonstrated with a below-20-nm half-pitch by employing a plasmonic bowtie nanoaperture (BNA) [3, 14]. The advances in nanoscale feature-size controllability and scalability allow NFL to be used for 1- to 2.5-dimensional surface nanofabrication [2, 3, 6, 15]. Furthermore, optical proximity correction methods have also been proposed to achieve high pattern fidelity control by adjusting the proximity effects caused by evanescent waves [16–18]. However, the previously reported experimental results suffer from a critical issue in terms of line edge roughness (LER) even over a small patterning area, which can limit the applications of NFL [2, 3, 6, 16, 19, 20].

LER indicates the surface roughness of developed pattern features, and it cannot be automatically scaled down with the decrease in the feature size because it can significantly degrade the performance of semiconductor devices and limit the practical lithographic resolution and fidelity as the feature size decreases [21–26]. Hence, the quantitative evaluation and reduction of LER are required as a highly influential process for nanoscale patterning. Many lithography techniques such as conventional optical lithography, electron-beam lithography, extreme ultraviolet (EUV) lithography, and He ion beam lithography, as

well as other techniques, have made a great deal of efforts on these LER requirements via experiments, simulations, and approximate calculations [27–33]. Previous studies have found that LER is caused by a series of stochastically fluctuating effects [30, 34].

Typically, LER is widely used as an important factor for the evaluations of lithographic performance and pattern uniformity in NFL [2, 13, 16]. Unfortunately, the measured LER is experimentally demonstrated to be far from patterning targets with features beyond 20 nm. Therefore, analyzing the causes and predicting the value of LER are critical to achieving high pattern quality in real-world applications. However, the LER generation mechanism in the NFL has not yet been intensively studied. In NFL with a ridge nanoaperture, a laterally propagating wave including QSWs and SPPs exhibits decay rate in the *x*-, *y*-, and *z*-directions. Given that LER is affected by the image log-slope (ILS) at the line pattern edge [35], field attenuation in the lateral direction needs to be considered when analyzing LER in NFL. The point-spread function (PSF) of the photoresist (PR) can be employed to quantitatively extract the lateral decay constant [33, 36–37]. For a realistic patterning process, the patterning feature at the edge position also suffers from a lower PR contrast with the decrease in size; this results from the low ILS and the energy loss due to the optical absorption of the PR [38–39].

In the present study, we investigate the effect of the decay characteristics of evanescent waves on the ILS and PR contrast and further clarify the generation mechanism of LER in NFL using a plasmonic bowtie-shaped nanoaperture. For accurate and reliable estimation of the LER, the PR PSF is measured in the lateral direction of the generated spot-mapping pattern, and the line-spread function (LSF) is computed by the convolution of the dose distribution of a line image with the PR PSF. The decay constant is extracted from the measured PSF and LSF to estimate the PR contrast in the NFL using a proposed analytic formula, which is deduced from the formula of the PR contrast in far-field optical lithography. We introduce an experimentally validated analytical model for LER in NFL. LER is analytically estimated as a function of the exposure dose, PR contrast, and ILS. We find that LER generation is a complicated stochastic process, and more importantly, the decaying feature of the surface waves plays a noticeable role in this generation. The dominance of the evanescent field is further experimentally and theoretically investigated by increasing the ILS via control of the gap size. These analyses are expected to provide useful guidance in minimizing the feature errors and effectively enhancing the pattern uniformity in the near-field nanopatterning process.

2 Modeling

2.1 Effects of the decaying feature on ILS and photoresist contrast

A schematic of the near-field nanopatterning process with a plasmonic contact probe is shown in Figure 1A. Compared with conventional optical lithography, whose pattern is generated by diffraction of the far field, the lateral dimension of the pattern in NFL is determined by laterally propagating QSWs and SPPs with large decaying features. Because LER is related to ILS and ILS can be evaluated by field distribution in the *xy*-plane without considering the decay rate in the *z*-direction, we adopt the evanescent mode of the QSW and SPP for LER calculation. Accordingly, a critical step to fully capture the effect of near-field distribution on the pattern quality is to quantify the PR PSF. Extraction of the PR PSF from spot-mapping patterns using a calibration process has been demonstrated, and it plays an important role in the pattern profile prediction [5–6]. However, LER is related to the edge roughness of the line patterns, which means that LER generation is mainly affected by the outermost edge field distribution at the exit of the plasmonic BNA. For a plasmonic BNA, as the quality of the focused beam spot at its exit plane is strongly dependent on the polarization direction of the illumination laser [40–41], a transverse magnetic polarized laser at 405 nm was employed to obtain extremely high transmission and optical resolution, as shown in Figure 1A–C. Hence, the transmitted intensity at the maximum width in the *y*-direction determined by the surface waves plays an important role in LER generation along the *x* scanning direction.

For a large pattern where the pattern size is approximately half of the incident wavelength, decay rate *q* of the QSW is higher than that of the spherical wave. However, for a pattern size that is smaller than 0.1 of the wavelength, the pattern is mainly recorded by the intensity near the aperture. In the vicinity of the aperture, decay rate *q* of the QSW converges to 1, which implies that the decay rate of the QSW is the same as that of the spherical wave. Consequently, the QSW intensity decreases at $1/\rho^2$. We further revise the analytical formula of the PR PSF reported in [5] as follows:

$$D_{\mathrm{psf}}(\rho,\varphi)=\left(\frac{A_{\mathrm{QSW}}^2}{\rho^2}+\frac{A_{\mathrm{SPP}}^2}{\rho}+\frac{A_{\mathrm{QSW}}A_{\mathrm{SPP}}}{\rho\sqrt{\rho}}\cos(\phi-\delta)\right)(\cos^2\varphi)t, \quad (1)$$

where the PR PSF is denoted by $D_{\mathrm{psf}}(\rho,\varphi)$. It is a function of the lateral length $\rho=(x_m^{\,2}+y_m^{\,2})^{1/2}$ and $\varphi=\cos^{-1}(x_m/\rho)$.

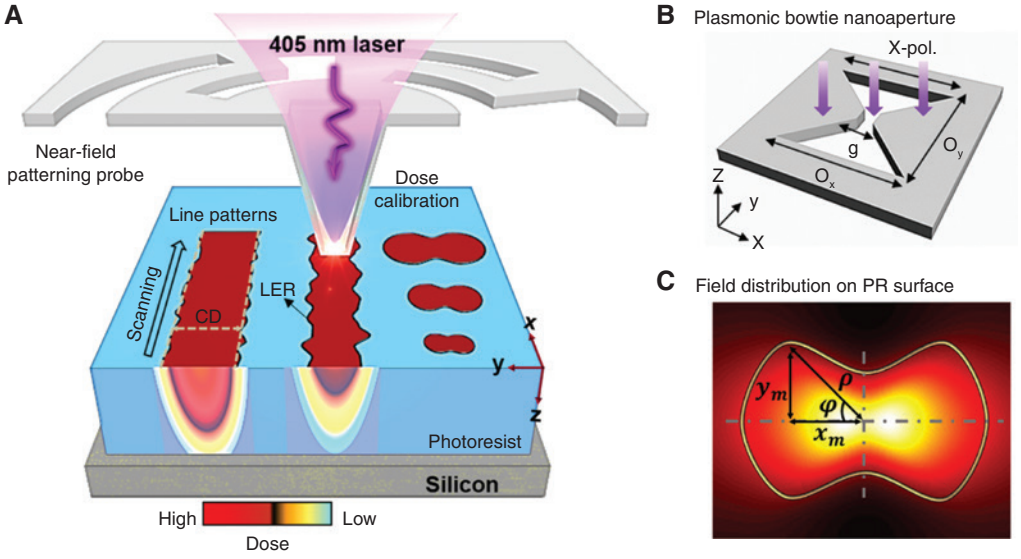

Figure 1: Schematics of the near-field patterning process using a scanning plasmonic BNA.
(A) Dose calibration using spot-mapping patterns to extract the decay characteristics of the evanescent field. LER analysis of the line patterns was carried out with different CDs by adjusting the exposure-dose distributions on the photoresist surface. The optical source, which is a linearly *x*-polarized laser with 405 nm wavelength, is incident on a metallic BNA. (B) Geometry of a plasmonic BNA, which is perforated at the tip apex of the near-field patterning probe in (A). The outline dimension is $O_x = O_y = 150$ nm with various ridge-gap sizes (g) from 10 to 30 nm. (C) Calculated field distribution excited by a plasmonic BNA on the photoresist surface and geometry of the photoresist PSF.

y_m is half of the top critical dimension (CD) of the maximum width in the *y*-direction, and x_m is its corresponding coordinate in the *x*-direction, as shown in Figure 1C. The cosine term originates from the dipole radiation of the local plasmon, where A_{QSW} and A_{SPP} are the field amplitudes of the evanescent mode of the QSW and SPP, respectively. $\phi - \delta$ is a possible phase delay between the QSW and SPP (more details of the derivation process of Eq. (1) are shown in Supplementary Section S1).

Because of the inherent characteristic of the evanescent waves, the local dose distribution $D_{psf}(\rho, \varphi)$ can be expressed with an exponential decay function [2, 42]. To obtain a simple analytic decay function for the PR PSF, we assume that the decay constant at the edge position is approximated by the linear function $\beta(\rho) = a + b\rho$, where a is the decay constant at $\rho = 0$, and b is a dimensionless parameter [2]. The constants a and b depend on the spatial distribution of $D_{psf}(\rho, \varphi)$, and can be obtained by fitting the local dose at the edge position of Eq. (1). For line patterns, owing to the optical proximity effects, i.e. the overlap of the PR PSFs, the decay constant can be extracted using the convolutional relationship between the PSF and LSF (see Eq. (S5)). By comparing the exposure dose profiles of the line patterns in far-field lithography (FFL) and NFL, as schematically shown in Figure 2, the rapid decay of the evanescent field at the edge position can result in a decreased ILS. It should be noted that the small ILS caused by the decay of the evanescent field can cause the LER-generation region to be larger than that in FFL.

The PR contrast, which is simultaneously affected by the exposure and post-exposure processes, plays a paramount role in LER generation because it determines the PR residues at the edge positions. However, as the near-field around the plasmonic nanoaperture rapidly decays, the PR contrast in NFL has been rewritten as a function of the decay property of the exposure beam and the absorption coefficient of the used PR [2]. Thus, to further study the LER generation mechanism in the NFL, the generated PR contrast needs to be quantitatively compared with that in FFL. However, in practical applications, no theoretical analysis or experimental measurement methods can be directly applied to separately estimate the PR contrast in the near and far fields. To solve this problem, on the basis of the common theory about PR contrast [2, 39], we divide the PR contrast in NFL into two categories, namely that associated with the far-field PR contrast γ_{far} (which depends on the energy loss caused by the PR absorption that exists in all lithography techniques), and the evanescent-field-induced PR contrast γ_{decay} (which depends on the decay constant (β) of the near field). Then, the PR contrast generated by NFL, γ_{near}, can be theoretically expressed as

$$\gamma_{near}^{-1} = \gamma_{far}^{-1} + \gamma_{decay}^{-1}. \quad (2)$$

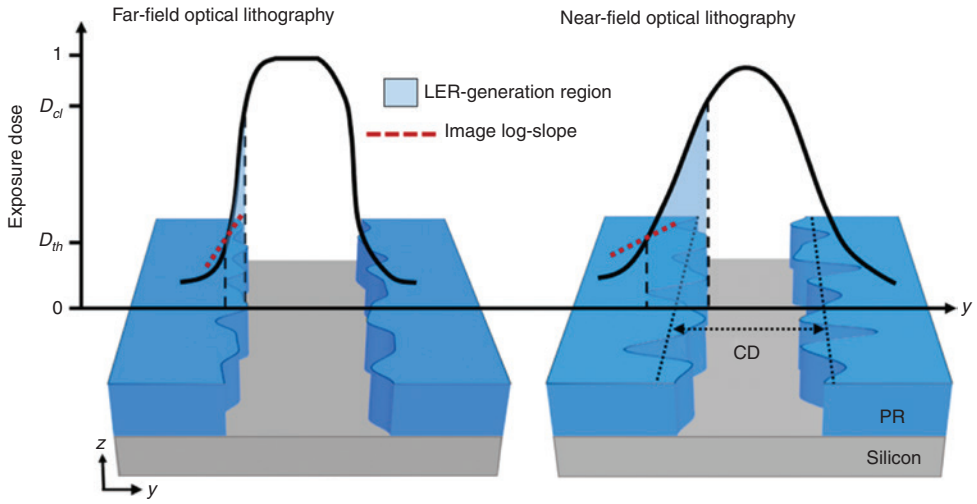

Figure 2: Schematic diagram showing the difference in LER generation in far- and near-field optical lithography.
The generated pattern profile depends on the threshold dose D_{th} and the clearing dose D_{cl}, which are defined as the minimum exposure doses for PR removal and the clearing doses for complete PR removal, respectively. The blue areas represent the LER generation regions. Its most significant contributor is the ILS, shown as red dotted lines. ILS is defined as the quantified profile steepness at the line edge position (i.e. the position of the full width at tenth maximum (FWTM) of the generated line profile). Note that the evanescent field can induce small ILS and thereby lead to a larger LER in NFL.

Equation (2) indicates that the effect of the evanescent field decay on the PR contrast can be separately determined (the derivation of Eq. (2) is described in detail in Supplementary Section S2). Because γ_{decay} is much less than γ_{far}, it yields a low γ_{near}. Generally, a larger PR contrast represents a higher pattern quality in the PR film [30]. Therefore, γ_{decay} can provide further support to our prediction that near-field decay will induce a large loss in the PR contrast, thereby increasing the LER. To confirm the validity of the analytical formula, we will use it to fit the measured PR contrast extracted from the PR contrast curve obtained from the experimental data. On the basis of the theoretical analysis, because the decay characteristics of the evanescent field can induce a small ILS and PR contrast loss in NFL, the causes of LER in NFL are essentially different from those in the other techniques.

2.2 LER modeling in NFL

A central issue in this work is finding an appropriate mathematical model to estimate the feature variation at the line edge position and thereby performing quantitative characterization of LER. Taylor series approximation is used to derive the local exposure-dose distribution $D(y)$, which can be expressed as $D(y)=D(y_i)+\frac{\partial D(y)}{\partial y}|_{y_i}(y-y_i)+\cdots$, where $\Delta y_i=(y-y_i)$. Here, y is the local position with a nominal CD, and y_i is the developed edge position measured at the ith point at the line edge (shown in Figure S3). For small values of Δy_i, i.e. smaller than 50 nm (larger than the measured LER value), the local dose distribution $D(y)$ can be a good approximation of the Taylor series expansion in the first order with an error of 8%. By applying the threshold dose condition to the exposure dose at y_i, we can obtain the resulting change Δy_i at the PR edge position, which can be approximately expressed as

$$\Delta y_i \cong \frac{D(y)-D(y_i)}{D_{th}}\left(\frac{1}{D_{th}}\frac{\partial D(y)}{\partial y}|_{y_i}\right)^{-1}=\frac{\Delta D_{ex}}{D_{th}}\left(\frac{1}{\text{ILS}}\right), \tag{3}$$

where $D(y_i)=D_{th}$ is the exposure dose at the feature edge, and $\frac{\partial D(y)}{\partial y}|_{y_i}$ is the local gradient of the exposure dose at the edge position. ILS is calculated as a function of $\left(\frac{1}{D(y_i)}\frac{\partial D(y)}{\partial y}|_{y_i}\right)$. ΔD_{ex} denotes the dose fluctuation $(D(y)-D(y_i))$ at the line edge position. For some variations in exposure dose $\sigma_{D_{ex}}$, $\sigma_{\text{LER}}=\frac{\sigma_{D_{ex}}}{D_{th}}\left(\frac{1}{\text{ILS}}\right)$; thus, the resulting LER can be expressed as follows:

$$3\sigma_{\text{LER}}=\frac{3}{\sqrt{D_{\text{nor}}}}e^{\frac{1}{\gamma_{\text{near}}}}\left(\frac{1}{\text{ILS}}\right). \tag{4}$$

Here, D_{nor} is the normalized exposure dose, and γ_{near} represents the PR contrast at the line edge position (more details of the derivation of Eqs. (3) and (4) are shown in Supplementary Section S4).

According to Eq. (4), we know that there are several sources of LER in NFL; the exposure dose variation, PR material properties, and aerial image quality all contribute to the total LER of the final pattern feature. Note that the causes of LER generation in NFL are different from those in EUV lithography, where the photon shot noise (PSN) is the significant contributor to LER. The PSN contribution to LER can be ignored in NFL, as the number of the photons absorbed near the edge feature in NFL is over 25 times more than that in EUV lithography when the PRs used have the same sensitivity. The exposure variations can be considered as random fluctuations in the patterning process, which can be modeled using Poisson statistics, and yield the standard $1/\sqrt{\text{Dose}}$ dependence observed in essentially all LER models [30].

3 Results and discussion

3.1 Decay characteristics extraction in the evanescent field

The pattern feature is determined by the exposure-dose distribution on the PR depending on the complicated decay characteristics of the evanescent field. Thus, the decay constant of the evanescent field can be extracted from the experimental result. Spot-mapping patterns were recorded on a positive PR (Dongjin Semichem, DPR i-7201) using a direct-writing laser lithographic system and a NFL system with a nanoscale bowtie aperture. A 100-nm-thick PR was deposited on a Si wafer using the spin-coating method. The spot-mapping patterns were generated with exposure times ranging from 1 to 12 ms under a fixed laser power, followed by cold KOH development (at a temperature of approximately –10°C). The developed feature sizes of the spot-mapping patterns were measured using atomic force microscopy (AFM; Park systems, XE-100) in a noncontact mode. The AFM image of the generated spot pattern is shown in the inset in Figure 3A.

Comparison with the calculated field distribution shown in Figure 1C revealed that the spatial distribution of the near field through a plasmonic BNA could be quantitatively mapped using the spot patterns. The PR PSF was defined as a function of the lateral length ρ, which was normalized to D_{th} to compare the measured PR PSFs without the effect of different PR sensitivities under these exposure energies (see Eq. (S4)). The plot of the normalized PR PSFs versus the spot lateral length (ρ) is shown in Figure 3A. The solid line in Figure 3A is the theoretical D_{psf} profile generated by the plasmonic BNA. The residual errors between the measured PR PSFs and the fitted values were estimated to be within ±0.002. It shows that the proposed PR PSF formula agrees well with the experimental data. From the fitting process in Eq. (1), we obtained $A_{QSW} = 91.5763$, $A_{SPP} = -0.4387$, and the phase delay term of $\cos(\phi - \delta) = 0.4890$. The parameters a and b of the decay constant β were fitted as 17.0700 nm and 0.4148 from the PR PSF curve. Then, according to the estimated decay constant $\beta(\rho)$ determined by the PR PSF, the evanescent-field-induced PR contrast γ_{deacy} can be obtained (see the equations in Supplementary Section S2). The PR contrast

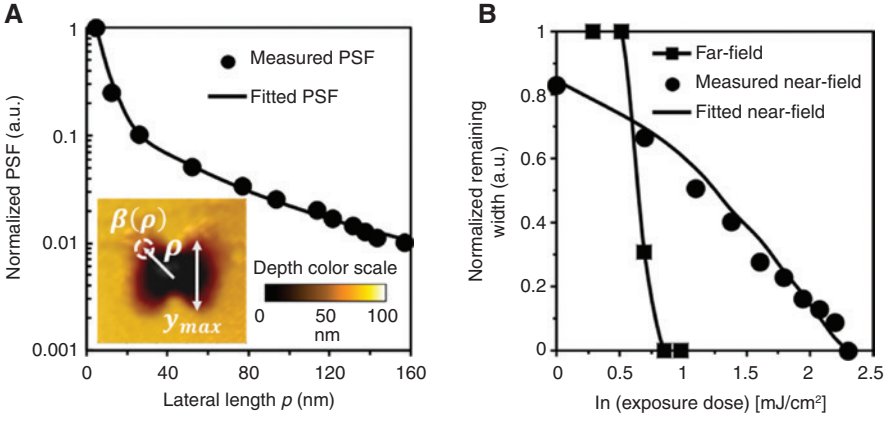

Figure 3: Normalized photoresist PSFs and photoresist contrast curves.
(A) Measured curve of the normalized photoresist PSFs obtained by analyzing the features of the (solid circles) spot-mapping patterns and (solid line) fitted curve of the normalized photoresist PSFs. Inset: AFM image of the generated spot pattern. y_{max} is the maximum width in the y-direction, ρ is the lateral length, and $\beta(\rho)$ is the corresponding decay constant with respect to ρ. (B) Photoresist contrast curve of (solid line with squares) far-field lithography, (solid circles) measured photoresist contrast curve of NFL, and (solid line) fitted photoresist contrast curve using the analytic formula of the photoresist contrast for NFL.

curves generated by FFL and NFL are shown in Figure 3B. The remaining width was the estimated top CD of the non-exposure linewidth for a positive PR, and it is analogous to the remaining thickness of PR contrast in the conventional FFL. By normalizing the remaining width and using the threshold dose model, we obtained the measured PR contrast as $\gamma = (\ln(D_{cl} / D_{th}))^{-1}$, and its value could be extracted from the PR contrast curve. The far-field PR contrast was estimated to be $\gamma_{far} \sim 3.7845$. On the other hand, the value of the near-field PR contrast was not fixed. It varied with different lateral lengths, $0.1703 \le \gamma_{near} \le 0.4595$. Figure 3B also shows that the estimated results obtained from Eq. (2) could fit well with the experimental results, with residual errors within ±0.07. These results indicated that the near-field PR contrast γ_{near} was significantly smaller than the far-field γ_{far} because of the loss induced by the rapid decay of the near-field. More importantly, the evanescent-field-induced PR contrast γ_{decay} implies that one of the most significant contributors to the LER in near-field nanopatterning is the PR contrast.

3.2 LER evaluation in the near-field nanopatterning

The main focus of our experiments was to estimate the LER versus feature size relationship and then determine an LER-reduction method based on the proposed approximate analytical solution. Because of the complicated proximity effects on the line patterns, i.e. the overlap of the PR PSFs is the main factor that determines the PR residue among features, an accurate measurement of the PR LSF is fundamental to modeling the LER in the near-field nanopatterning process. To measure the LSF in the PR, a sequence of line patterns at increasing exposure doses were generated using NFL with a plasmonic BNA while keeping the scanning speed at 0.5 mm/s. The used bowtie-shaped nanoaperture was fabricated using the focused-ion-beam milling method, which had a dimension of 150 nm × 150 nm with a 20-nm gap size, as shown in the inset of Figure 4B. After the development, the top CD of the exposed line patterns was measured using AFM.

Figure 4A shows the results of the measured and calculated normalized PR LSFs. The calculated LSFs obtained from Eq. (S5) are in good agreement with the measured LSFs. The ILS is also plotted as a function of the feature size in Figure 4A. To confirm the feasibility of Eq. (4), the estimated LER was compared with the measured LER from the experimental pattern results. The LERs of the line patterns from the top-view images of the developed pattern profiles with various top CDs were analyzed using software developed in-house. The resulting pitch-dependent LER is shown in Figure 4B, which confirms that the calculation results of the analytical model and the experimental results match well with a small fitting error. This result shows that Eq. (4) can be used to theoretically predict the LER of NFL at various feature sizes. Figure 4B and C show that the LER of NFL increased with the decrease in the feature size because the ILS, PR contrast, and the required exposure dose decreased, resulting in serious pattern collapse, division, residuals, or height reduction. Thus, a LER reduction method is highly needed to meet the LER-reduction requirement. Note that as the feature size continuously increased by more than 150 nm, the measured LER saturated at ~9.1 ± 0.8 nm. After the saturation point, any increase in the exposure dose had no effect on the improvement of the LER. Therefore, we believe that the saturated LER mainly originated from the limitation of the experimental conditions, such as the intrinsic material characteristics of the used PR and the developer. The proposed LER estimation method for NFL as an experiment-based model can effectively predict the generated LER.

LER reduction is another very crucial chanllenge to be addressed in advanced nanotechnology nodes. In order to achieve LER minimization in NFL, the effects of ILS on the generated LER were experimentally observed and theoretically analyzed. Because the gap size between the ridges of the plasmonic BNA determines its near-field localization, ILS can be controlled via the gap size, thereby influencing LER generation. The relative relationship of the ILS among the gap sizes of 10, 17, 20, and 30 nm were used to calculate the LER generated by these gap sizes with 1 mm/s scanning speed while keeping the development conditions constant. The comparison result of the predicted and measured LERs is plotted with the gap size and shown in Figure 5A. Figure 5B shows the AFM images of the line patterns with a 100-nm feature generated using probes with gap sizes of 10 and 20 nm. The experimental results again demonstrate that the rapidly decaying evanescent field is a dominant optical contributor to LER generation because the smaller the effect of the evanescent field on the ILS, the smaller is the LER. The results also reveal that the generated LER can definitely meet the standard of LER requirements when the NFL system produces a sufficiently good quality of the aerial image.

When an *x*-polarized light is incident on the metallic bowtie-shaped nanoaperture, which is a type of ridge aperture that exploits the gap plasmon, the field confinement factor and field distribution strongly depend on the gap size [43–45]. To further understand the relationship between the gap size and the ILS and their impact on LER

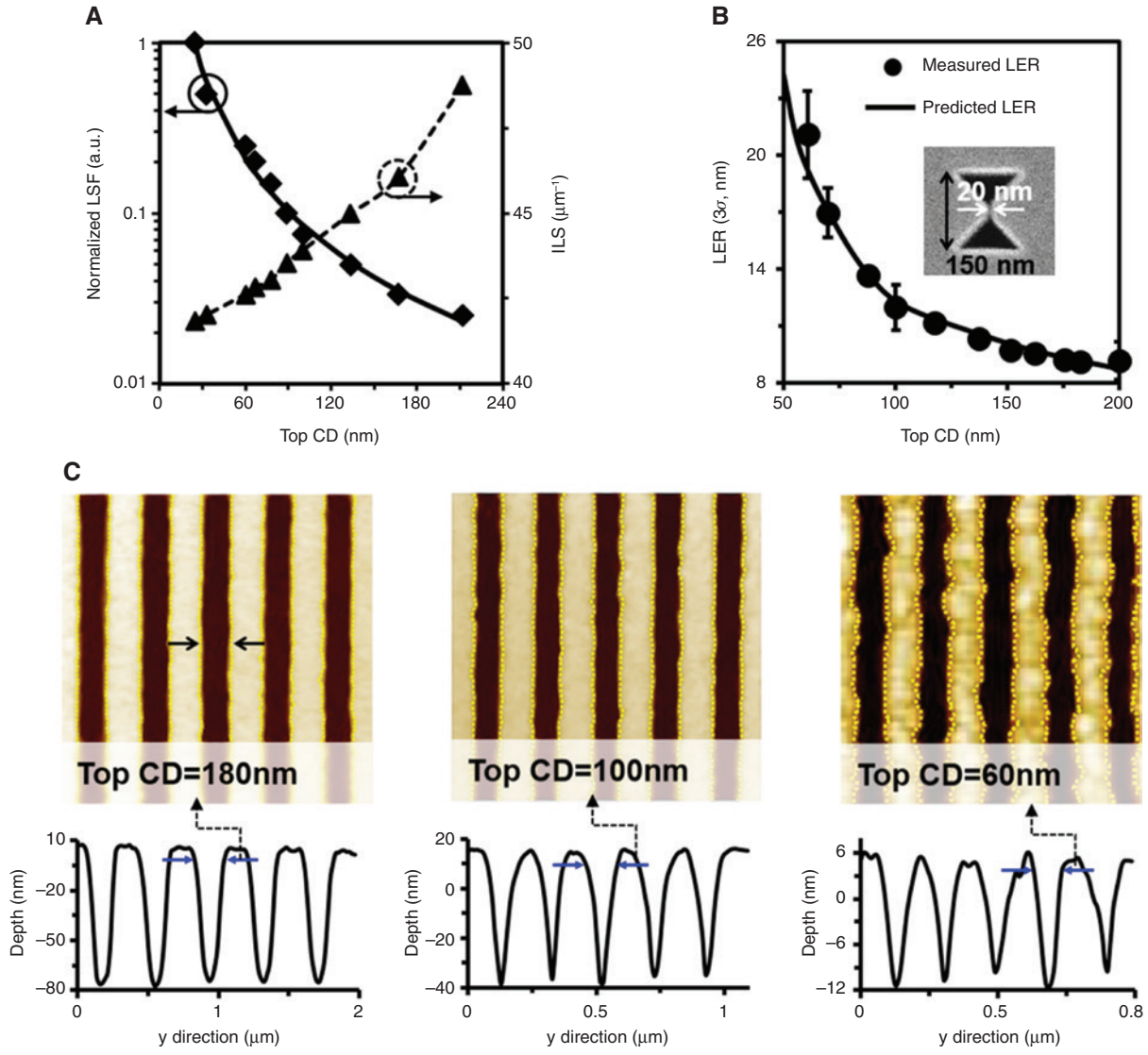

Figure 4: LER estimation and characterization.
(A) Comparison of the (solid diamonds) measured and (solid line) calculated LSFs of the photoresist obtained using the convolutional relationship between the photoresist PSF and a line image and the calculated ILS as a function of feature size. (B) LER as a function of the top CD of the generated line pattern. (Solid circles) Measured and (solid line) predicted LERs. The error bars show the standard deviations (<3%) of the measured LERs. The inset shows the scanning electron microscopy(SEM) image of the used bowtie-shaped nanoaperture. (C) AFM images of the line patterns with various top CDs (the black arrows show the measured top CD). The generated LER is very clearly dependent on the feature size.

generation, we obtained the distributions of the electric field intensity components with gap sizes varying from 5 to 50 nm by implementing the finite-difference time-domain method (FDTD; Lumerical Solutions Inc., ver. 8.12.590) simulations. For the numerical analysis, we used the permittivity of the Al metal film as –23.9819 + 4.9508i and PR (n = 1.7), and set the bowtie outline as 150 nm × 150 nm. The Al and PR thicknesses were 100 nm each. The total intensity distribution on the xz-plane is $I_{\text{total}} = |E_x + E_z|^2$, where E_x and E_z are the x and z component of the electric field, respectively. Because the ratio of the transmission amplitude of the two electric field components determines the pattern fidelity, a high ratio of $|E_x|^2/|E_z|^2$ is required to generate an aerial image with good contrast [13, 46]. The calculated intensity ratios $|E_x|^2/|E_z|^2$ for several plasmonic bowtie apertures with various gap sizes are shown in Figure 6A, which show that with decreasing gap size, a larger ratio of $|E_x|^2/|E_z|^2$ can be obtained, thus yielding an aerial image with higher quality. To further validate the gap-size-dependent field-coupling effect, the

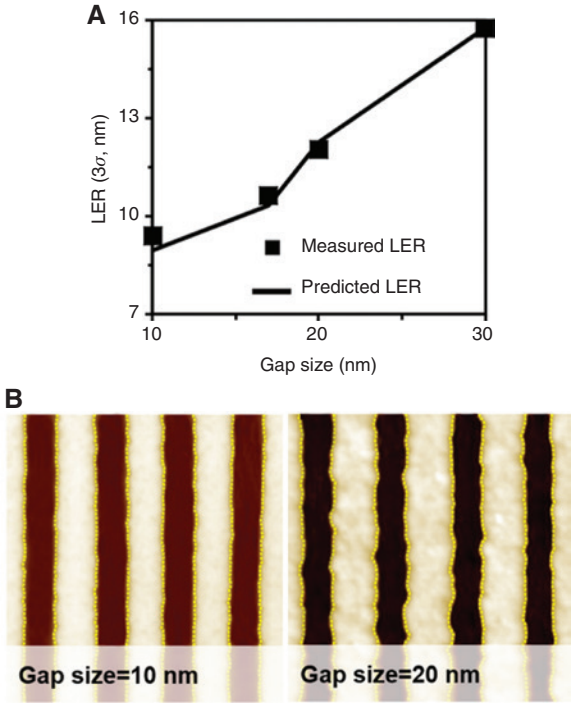

Figure 5: LER reduction by controlling the gap size. (A) Comparison results of the LER versus gap size between the (solid squares) measured and (solid line) predicted LERs. (B) AFM-measured profiles of the line patterns with a 100-nm top CD generated using two probes with gap sizes of 10 and 20 nm.

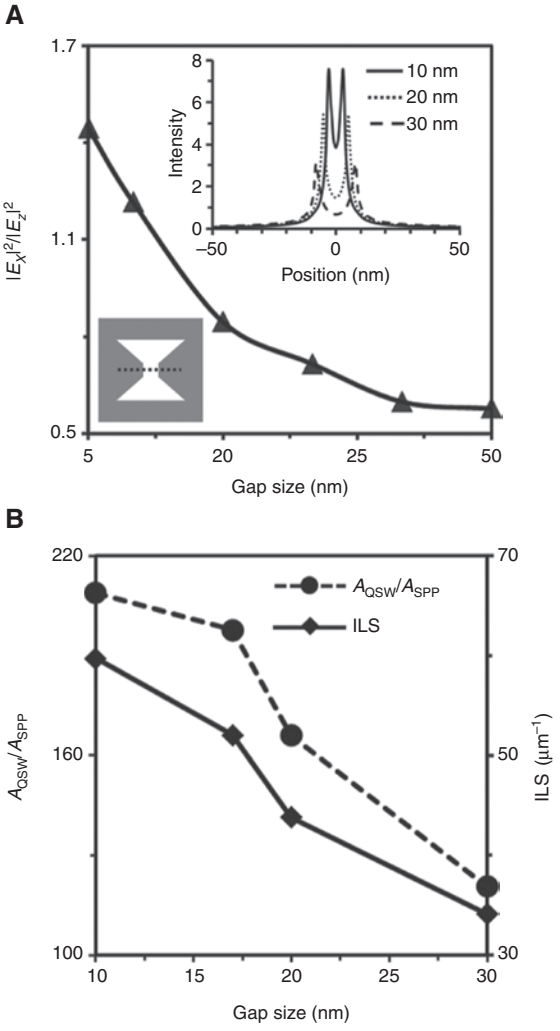

Figure 6: Effects of the gap size on the quality of the aerial image. (A) Calculated ratio $|E_x|^2/|E_z|^2$ as a function of the gap size. The inset shows the transmitted intensity profile through the different gap sizes at the gap center along the *x*-direction. (B) Calculated ratio A_{QSW}/A_{SPP} from the photoresist point-spread functions (PSFs) generated by the plasmonic BNA with gap sizes of 10, 17, 20, and 30 nm and calculated ILS as a function of the gap size at the edge position of the line patterns with a 100-nm top CD.

cross-sectional view of the intensity distribution (at the center of the ridge aperture along the *x*-direction on the PR surface) is shown in the inset of Figure 6A.

As the gap size becomes smaller, higher intensity can be achieved via the strong coupling of the plasmon-induced field. However, it strongly decays along the direction away from the two ridge edges of the bowtie-shaped aperture. The reason for this is that for a gap size smaller than $\lambda/10$, when the gap size becomes smaller, the SPP generation efficiency decreases, which implies that the influence of the evanescent field on the aerial image quality gradually weakens [47, 48]. To verify this conclusion, the ratio A_{QSW}/A_{SPP}, which can be approximately considered as the intensity ratio of the far- to the near-field component, is calculated from the PR PSF (i.e. Eq. (1)). The PR PSFs were obtained by the plasmonic BNA with gap sizes of 10, 17, 20, and 30 nm from the dose calibration processes. Figure 6B shows that the ratio A_{QSW}/A_{SPP} increases as the gap size decreases. Thus, the field ratio of the evanescent mode becomes smaller with the decrease in the gap size. Figure 6B also shows the calculated ILS with a 100-nm fixed top CD as a function of gap size by adjusting the PR PSFs. By comparing the variation tendency of the ratio A_{QSW}/A_{SPP} and ILS with the gap size, it is seen that they have almost the same relative relationship with respect to the gap sizes. Therefore, ILS can be enhanced by reducing the evanescent-field ratio generated by the SPPs via gap-size control, which yields low LER in the final pattern.

4 Conclusions

In this paper, we mainly discussed the physical concepts behind LER generation in NFL, and predicted the generated LER quantitatively using an approximate analytical

solution. We first investigated the effects of the decaying feature of the surface plasmon waves on the PR contrast. A PR PSF, which was determined by the evanescent model of the QSWs and SPPs, was employed to quantitatively analyze the effect of the decay characteristics in the lateral direction on LER generation in NFL. An analytical formula of the near-field PR contrast was further introduced to estimate the difference in the PR contrast between NFL and other lithography techniques. We demonstrated that the rapid decay of the evanescent field can induce a large loss in the PR contrast, leading to a high LER. For further study of the optical contributions to LER generation, FDTD simulations, in conjunction with the experimental results, were performed to determine the effects of the quality of an aerial image on the LER. We found that increasing the near-field component in the total fields can induce a reduction in the ILS and yield a large LER. The results presented in this paper have direct practical implications for a deeper understanding of LER generation in the near-field nanopatterning process. We expect that our findings and theoretical models will be useful for the quantitative evaluation of the final pattern fidelity with arbitrary shapes recorded using NFL-based nanofabrication.

5 Supplementary material

The supplementary material is available online on the journal's website or from the author.

Conflicts of interest: The authors declare no conflict of interest.

References

[1] Alkaisi MM, Blaikie RJ, McNab SJ. Nanolithography in the evanescent near field. Adv Mater 2001;13:877–87.
[2] Kim S, Jung H, Kim Y, Jang J, Hahn JW. Resolution limit in plasmonic lithography for practical applications beyond 2x-nm half pitch. Adv Mater 2012;24:337–44.
[3] Wen X, Datta A, Traverso LM, Pan L, Xu X, Moon EE. High throughput optical lithography by scanning a massive array of bowtie aperture antennas at near-field. Sci Rep 2015;5:16192.
[4] Wang L, Uppuluri SM, Jin EX, Xu X. Nanolithography using high transmission nanoscale bowtie apertures. Nano Lett 2006;6:361–4.
[5] Park C, Jung H, Hahn JW. Characterization of three-dimensional field distribution of bowtie aperture using quasi-spherical waves and surface plasmon polaritons. Sci Rep 2017;7:45352.
[6] Jung H, Park C, Oh S, Hahn JW. Nanoscale 2.5-dimensional surface patterning with plasmonic lithography. Sci Rep 2017;7:9721.
[7] Aigouy L, Lalanne P, Hugonin JP, Julié G, Mathet V, Mortier M. Near-field analysis of surface waves launched at nanoslit apertures. Phys Rev Lett 2007;98:153902.
[8] Gao P, Yao N, Wang C, et al. Enhancing aspect profile of half-pitch 32 nm and 22 nm lithography with plasmonic cavity lens. Appl Phys Lett 2015;106:093110.
[9] Zhao Z, Luo Y, Zhang W, et al. Going far beyond the near-field diffraction limit via plasmonic cavity lens with high spatial frequency spectrum off-axis illumination. Sci Rep 2015;5:15320.
[10] Wu J, Yu C, Li S, et al. Parallel near-field photolithography with metal-coated elastomeric masks. Langmuir 2015;31:1210.
[11] Chen X, Yang F, Zhang C, Zhou J, Guo LJ. Large-area high aspect ratio plasmonic interference lithography utilizing a single high-k mode. ACS Nano 2016;10:4039–45.
[12] Ji J, Meng Y, Hu Y, Xu J, Li S, Yang G. High-speed near-field photolithography at 16.85 nm linewidth with linearly polarized illumination. Opt Express 2017;25:17571–80.
[13] Liang G, Chen X, Zhao Q, Guo LJ. Achieving pattern uniformity in plasmonic lithography by spatial frequency selection. Nanophotonics 2018;7:277–86.
[14] Chen Y, Qin J, Chen J, et al. 16 nm-resolution lithography using ultrasmall-gap bowtie apertures. Nanotechnology 2017;28:055302.
[15] Kim Y, Jung H, Kim S, Jang J, Lee JY, Hahn JW. Accurate near-field lithography modeling and quantitative mapping of the near-field distribution of a plasmonic nanoaperture in a metal. Opt Express 2011;19:19296–309.
[16] Oh S, Han D, Shim HB, Hahn JW. Optical proximity correction (OPC) in near-field lithography with pixel-based field sectioning time modulation. Nanotechnology 2018;29:045301.
[17] Wang C, Gao P, Zhao Z, et al. Deep sub-wavelength imaging lithography by a reflective plasmonic slab. Opt Express 2013;21:20683–91.
[18] Luo Y, Liu L, Zhang W, et al. Proximity correction and resolution enhancement of plasmonic lens lithography far beyond the near field diffraction limit. RSC Adv 2017;7:12366–73.
[19] Graham JL. Light-directed nanosynthesis: near-field optical approaches to integration of the top-down and bottom-up fabrication paradigms. Nanoscale 2012;4:1840–55.
[20] Jun L, Bo Z, Changtao W, et al. Fabrication of anisotropically arrayed nano-slots metasurfaces using reflective plasmonic lithography. Nanoscale 2015;7:18805–12.
[21] Jiang Z, Cheng H, Blakey I, Whittaker AK. Healing surface roughness of lithographic nanopatterns through sub-10 nm aqueous-dispersible polymeric particles with excellent dry etch durability. Mol Syst Des Eng 2018;3:627–35.
[22] Germack DS, Checco A, Ocko BM. Directed assembly of P3HT:PCBM blend films using a chemical template with sub-300 nm features. ACS Nano 2013;7:1990–9.
[23] Liddle JA, Gregg MG. Lithography, metrology and nanomanufacturing. Nanoscale 2011;3:2679–88.
[24] Mojarad N, Hojeij M, Wang L, Gobrecht J, Ekinci Y. Single-digit-resolution nanopatterning with extreme ultraviolet light for the 2.5 nm technology node and beyond. Nanoscale 2015;7:4031–7.
[25] Yinyong L, Jaewon C, Zhiwei S, Thomas PR, Kenneth RC. Fabrication of sub-20 nm patterns using dopamine chemistry in self-aligned double patterning. Nanoscale 2018;10:20779–84.

[26] Yamaguchi A, Tsuchiya R, Fukuda H, Komuro O, Kawada H, Iizumi T. Characterization of line-edge roughness in resist patterns and estimation of its effect on device performance. Proc SPIE 2003;5038:689–98.
[27] Saeki A, Kozawa T, Tagawa S, Cao HB, Deng H, Leeson MJ. Line edge roughness after development in a positive-tone chemically amplified resist of post-optical lithography investigated by Monte Carlo simulation and a dissolution model. Nanotechnology 2008;19:015705.
[28] Guo R, Lee S, Choi J, et al. Analytic estimation of line edge roughness for large-scale uniform patterns in electronbeam lithography. J Vac Sci Technol B 2016;34:06K605–9.
[29] Chang E, Mikolas D, Lin P, et al. Improving feature size uniformity from interference lithography systems with non-uniform intensity profiles. Nanotechnology 2013;24:455301.
[30] Mojarad N, Gobrecht J, Ekinci Y. Beyond EUV lithography: a comparative study of efficient photoresists' performance. Sci Rep 2015;5:9235.
[31] Ashby PD, Olynick DL, Ogletree DF, Naulleau PP. Resist materials for extreme ultraviolet lithography: toward low-cost single-digit-nanometer patterning. Adv Mater 2015;27:5813–9.
[32] Fukuda H. Analysis of line edge roughness using probability process model for chemically amplified resists. Jpn J Appl Phys 2003;42:3748–54.
[33] Winston D, Manfrinato VR, Nicaise SM, et al. Neon ion beam lithography (NIBL). Nano Lett 2011;11:4343–7.
[34] Kozawa T, Santillan JJ, Itani T. Analysis of stochastic effect in line-and-space resist patterns fabricated by extreme ultraviolet lithography. Appl Phys Express 2013;6:026502.
[35] Kozawa T, Tagawa S. Normalized image log slope with secondary electron migration effect in chemically amplified extreme ultraviolet resists. Appl Phys Express 2009;2:095004.
[36] Manfrinato VR, Wen J, Zhang L, et al. Determining the resolution limits of electron-beam lithography: direct measurement of the point-spread function. Nano Lett 2014;14:4406–12.
[37] Manfrinato VR, Zhang L, Su D, et al. Resolution Limits of electron-beam lithography toward the atomic scale. Nano Lett 2013;13:1555–8.
[38] Tobing LYM, Tjahjana L, Zhang DH. Direct patterning of high density sub-15 nm gold dot arrays using ultrahigh contrast electron beam lithography process on positive tone resist. Nanotechnology 2013;24:075303.
[39] Lee E, Hahn JW. The effect of photoresist contrast on the exposure profiles obtained with evanescent fields of nanoapertures. J Appl Phys 2008;103:083550.
[40] Jin EX, Xu X. Plasmonic effects in near-field optical transmission enhancement through a single bowtie-shaped aperture. Appl Phys B 2006;84:3–9.
[41] Huang Y, Liu L, Wang C, Chen W, Liu Y, Li L. Plasmonic direct writing lithography with a macroscopical contact probe. Appl Surf Sci 2018;441:99–104.
[42] Fleischer M, Bargioni AW, Altoe MVP, et al. Gold nanocone near-field scanning optical microscopy probes. ACS Nano 2011;5:2570–9.
[43] Ding L, Qin J, Guo S, Liu T, Kinzel E, Wang L. Resonant effects in nanoscale bowtie apertures. Sci Rep 2016;6:27254.
[44] Fang J, Tien C, Shieh HD. Hybrid-effect transmission enhancement induced by oblique illumination in nano-ridge waveguide. Opt Express 2007;15:11741–9.
[45] Kim M, Sim H, Yoon SJ, et al. Squeezing photons into a point-like space. Nano Lett 2015;15:4102.
[46] Guo X, Du J, Guo Y. Large-area surface-plasmon polariton interference lithography. Opt Lett 2006;31:2613.
[47] Lalanne P, Hugonin JP, Rodier JC. Theory of surface plasmon generation at nanoslit apertures. PRL 2005;95:263902.
[48] Beijnum FV, Rétif C, Smiet CB, Liu H, Lalanne P, van Exter MP. Quasi-cylindrical wave contribution in experiments on extraordinary optical transmission. Letter 2012;492:411–4.

Supplementary Material: The online version of this article offers supplementary material (https://doi.org/10.1515/nanoph-2019-0031).